Control Structure for Single-Phase Stand-Alone Wind-Based Energy Sources

Luminita Barote, *Member, IEEE*, Corneliu Marinescu, *Member, IEEE*, and Marcian N. Cirstea, *Senior Member, IEEE*

***Abstract*—This paper is analyzing the operation of a stand-alone wind turbine system with variable-speed permanent-magnet synchronous generator (PMSG) and a system for storing energy during wind speed and load variations. Energy storage devices are required for power balance and power quality in stand-alone wind energy systems. Initially, the holistic model of the entire system is achieved, including the PMSG, the boost converter, and the storage system. The power absorbed by the connected loads can be effectively delivered and supplied by the proposed wind turbine and energy storage systems, subject to an appropriate control method. The main purpose is to supply 230-V/50-Hz domestic appliances through a single-phase inverter. The simulation results, validated by experimental testing, show a good prediction of the electrical parameter waveforms. The control system is implemented on a dSPACE DS1103 real-time board. Furthermore, the results confirm the stability of the supply.**

***Index Terms*—Energy storage, real-time control, stand-alone generator, variable-speed permanent-magnet generators, wind power.**

I. Introduction

OVER THE past few years, research into the use of renewable energy sources (RESs), such as wind, photovoltaic, and hydropower plants [1]–[3], for electricity generation has been the subject of increased attention. In the case of wind energy conversion systems (WECSs), the interest is also focused on small units, used to provide electricity supply in remote areas that are beyond the reach of an electric power grid or cannot be economically connected to a grid. While large wind turbines reached their technological maturity, small-scale WECSs have to be further optimized in order to achieve integration in flexible microgrids (MGs) and increased reliability [4].

Clusters of MGs, linked through power and data exchange highways, play a similar role in the smart grid as the power generators do in classical power systems. However, the higher flexibility of the MGs and the easier integration of RES make them more attractive [5], [6]. WECSs are the most favored alternatives for supplying electricity in stand-alone cases at this moment due to the fact that wind energy is relatively easily harnessed, the maintenance required by the wind turbine generators is reasonable, and there is no fuel cost.

Several electrical machines can be used to implement the electromechanical energy conversion and control, each of which presents different advantages and disadvantages [7]–[9]. For small-power wind systems operating in remote and isolated areas, the study of permanent-magnet synchronous generators (PMSGs) has been the subject of much research. PMSGs are particularly interesting in low-power wind energy applications, due to their small size and high power density.

The primary advantage of PMSGs is that they do not require any external excitation current. A major cost benefit in using the PMSG is the fact that a diode bridge rectifier may be used at the generator terminals since no external excitation current is needed. The system topology used in this paper is based on a PMSG connected through a diode bridge rectifier and a boost converter to the dc link for small- and medium-power ranges [9]–[11].

Due to the highly variable nature of the wind, the utilization of an energy storage device such as a battery can significantly enhance the reliability of a small stand-alone wind system. Integrating an appropriate energy storage system in conjunction with a wind generator removes the fluctuations and can maximize the reliability of the power supplied to the loads [12]–[14]. In the autonomous system, the wind power converter may be operated to maximize the wind energy converted into electricity. The captured energy is supplied to the load directly, the difference between the wind power generation and user consumption being directed to or supplied by the battery energy storage device connected via the power electronic interface [2].

The lead–acid batteries (LABs) are the dominant energy storage technology, with their advantages of low price, high unit voltage, stable performance, and a wide range of operating temperature [15], [16]. The LABs hence constitute an exciting challenge, as major components in the development of the stand-alone wind energy systems [17], [18].

This paper is organized as follows. In Section II, the stand-alone wind turbine system configuration and associated control methods are presented; then, Section III describes the simulation and experimental results, while conclusions are provided in Section IV.

II. Stand-Alone Wind Turbine System Configuration

The proposed stand-alone wind power system supplies single-phase consumers at 230 V/50 Hz. It is designed for a residential location, and it is based on a 2-kW wind turbine

Manuscript received May 29, 2012; accepted June 14, 2012. Date of publication July 6, 2012; date of current version September 13, 2012. This work was supported by the European Social Fund and by the Romanian Government under project POSDRU/89/1.5/S/59323 through the Sectoral Operational Programme Human Resources Development.

L. Barote and C. Marinescu are with the Department of Electrical Engineering, Transilvania University of Braşov, 500024 Braşov, Romania (e-mail: luminita.barote@unitbv.ro; corneliu.marinescu@unitbv.ro).

M. N. Cirstea is with the Department of Computing and Technology, Anglia Ruskin University, CB1 1PT Cambridge, U.K. (e-mail: marcian@ieee.org).

Color versions of one or more of the figures in this paper are available online at http://ieeexplore.ieee.org.

Digital Object Identifier 10.1109/TIE.2012.2206346

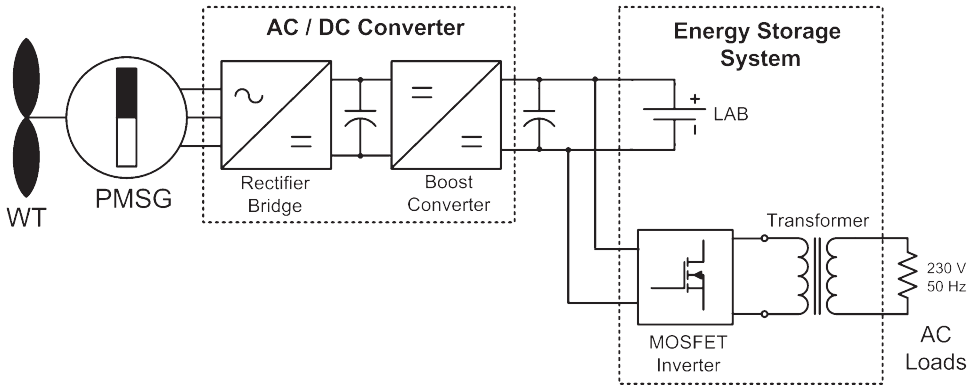

Fig. 1. Wind turbine configuration.

(Fig. 1), equipped with the following: 1) a direct-driven PMSG; 2) an ac/dc converter (diode rectifier bridge + boost converter) for the tracking of the maximum power from the available wind resource; 3) a LAB storage device; 4) an inverter; 5) a transformer; and 6) resistive loads. The wind power is converted into the mechanical rotational energy of the wind turbine rotor. A wind turbine cannot "completely" extract the power from the wind. Theoretically, only 59% of the wind power could be utilized by a wind turbine [19], but for the 2-kW wind turbine system analyzed in this paper, the real power coefficient is 39%.

The wind turbine rotor is connected to the wind generator, thus converting the mechanical energy into electrical energy. The generator's ac voltage is converted into dc voltage through an ac/dc converter. The rectifier is matching the generator's ac voltage to the dc voltage, while the boost converter provides the required level of constant dc voltage. The dc output voltage is fed to the battery bank and through an inverter further to the load. The voltage should stay constant for various wind speeds. When the wind speed is too high, the power excess supplied by the wind turbine is stored in the battery. When the wind speed is low, the generator, together with the battery bank, can provide sufficient energy to the loads. The dc loads are supplied directly from the dc circuit. At high speeds, the turbine control system stops the energy production. The same protection is activated also in the case when the battery is fully charged and energy production exceeds consumption. At low wind speeds, load shedding is used to keep the frequency at the rated value.

The storage system is composed of a LAB and a full-bridge single-phase inverter that converts the dc voltage of the battery to ac voltage. Furthermore, this voltage is applied to a single-phase transformer, which boosts up the voltage to 230 V. The inverter controls the power transfer.

A. PMSG Model

The dynamic model of PMSG is derived from the two-phase synchronous reference frame in which the q-axis is 90° ahead of the d-axis, with respect to the direction of rotation. The electrical model of PMSG in the synchronous reference frame is given by (1) [20]–[22]

$$\begin{cases} \frac{di_d}{dt} = -\frac{R_a}{L_d} i_d + \omega_e \frac{L_q}{L_d} i_q + \frac{1}{L_d} v_d \\ \frac{di_q}{dt} = -\frac{R_a}{L_q} i_q - \omega_e \left(\frac{L_d}{L_q} i_d + \frac{1}{L_d} \Psi_{PM} \right) + \frac{1}{L_q} v_q \end{cases} \tag{1}$$

where subscripts d and q refer to the physical quantities that have been transformed into the d–q synchronous rotating reference frame; R_a is the armature resistance; ω_e is the electrical rotating speed which is related to the mechanical rotating speed of the generator as $\omega_e = n_p \cdot \omega_g$, where n_p is the number of pole pairs; and $\psi_{\rm PM}$ is the magnetic flux of the permanent magnets. The electromagnetic torque can be derived, as shown in [23], to be

$$T_e = 1.5 n_p \cdot \left[(L_d - L_q) i_d i_q + \psi_{PM} i_q \right]. \tag{2}$$

If the PMSG is taken without rotor saliency (where $L_d = L_q = L$), (1) can be rewritten as

$$\begin{cases} \frac{di_d}{dt} = -\frac{R_a}{L} i_d + \omega_e i_q + \frac{1}{L} v_d \\ \frac{di_q}{dt} = -\frac{R_a}{L} i_q - \omega_e \left(i_d + \frac{1}{L} \Psi_{\rm PM} \right) + \frac{1}{L} v_q \end{cases} \tag{3}$$

and the electromagnetic torque can be regulated by i_q as

$$T_e = 1.5 n_p \psi_{\rm PM} i_q. \tag{4}$$

B. Boost Converter Model

The unidirectional boost converter achieves an interface between the battery and the rectifier capacitor and ensures the rapid transfer of power [24]. The block diagram is shown in Fig. 2(a), and a simplified model of the boost converter is shown in Fig. 2(b).

The voltage and current relationship between the primary and secondary sides is given by (5) and (6)

$$V_b = \frac{V_{\rm dc}}{1 - D} \tag{5}$$

$$I_b = I_{\rm Lconv} (1 - D) \tag{6}$$

where D is the pulse-width modulation (PWM) modulation factor.

When $V_{\rm dc} \geq V_b$, the boost converter is not working, and the current provided by the generator is channeled through the bypass Schottky diode D_s. In (5) and (6), it is assumed that there is no power loss in the converter. The input and output signals of the boost converter are modeled by two controlled current sources [see Fig. 2(b)].

The reference current $(I^*_{\rm Lconv})$ is supplied by the maximum power point tracking (MPPT). The error between the reference current and the measured current $(I_{\rm Lconv})$ is applied to a

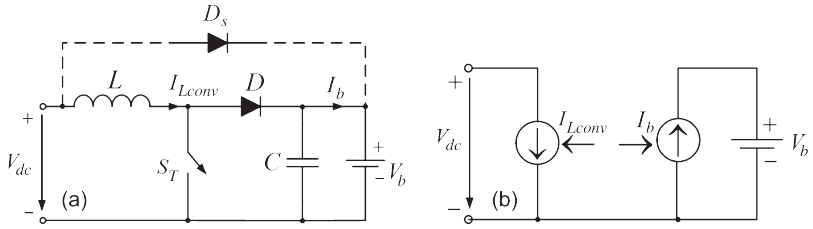

Fig. 2. (a) Boost converter diagram. (b) Equivalent model of the boost converter.

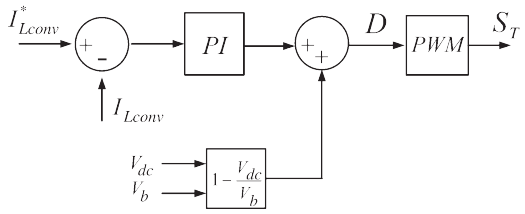

Fig. 3. Boost converter control diagram.

proportional integrator (PI) regulator. The output of the regulator is summed with the positive voltage reaction, which realizes $1\ V_{\rm dc}/V_b$. The modulation factor D is obtained, which is used as a reference for the PWM generator, as shown in Fig. 3. The modulation factor provides the control signal for the converter's switching device S_T.

In order to control the generator current and to provide overspeed limitation, our research team proposed in [25] a control method which is applicable to the dc boost converter block diagram analyzed (see Fig. 2). Also, the operation of the PMSG rectifier is characterized by variable frequency and variable voltage, as the wind turbine rotor speed varies.

C. MPPT

To obtain maximum power from a controlled WECS, this has to operate in the variable-speed mode. Thus, an adequate controlling method, based on MPPT, must be used, in order to maximize the electric output power and to adjust the generator speed [12], [13], [26].

Several studies have been dedicated to small turbines, including different architectures with their associated complexity and implementing different control strategies giving certain energy efficiency values. Knowing the optimal characteristics allows maximizing the energy transfer by controlling the torque, speed, or power. In fact, energy efficiency not only depends on the control strategy but is also influenced by the system topology and its losses [26].

Depending on the wind speed, the MPPT control adjusts the power transferred, bringing the turbine operating points onto the "maximum power curve," like in Fig. 4(a). In the case of the system studied, both in the simulations and in the experiments, the converter control system did not allow obtaining maximum power over the entire range of wind speeds, but only from 3 to 6 m/s, due to current limitations introduced by the motor inverter which emulated the wind turbine. A PI regulator is used to implement the MPPT function, which provides the reference power for the boost converter, based on the wind speed measurements $(v_{\rm p.u.})$ and the turbine generator speed $(n_{\rm p.u.})$.

The MPPT control block diagram is shown in Fig. 4(b).

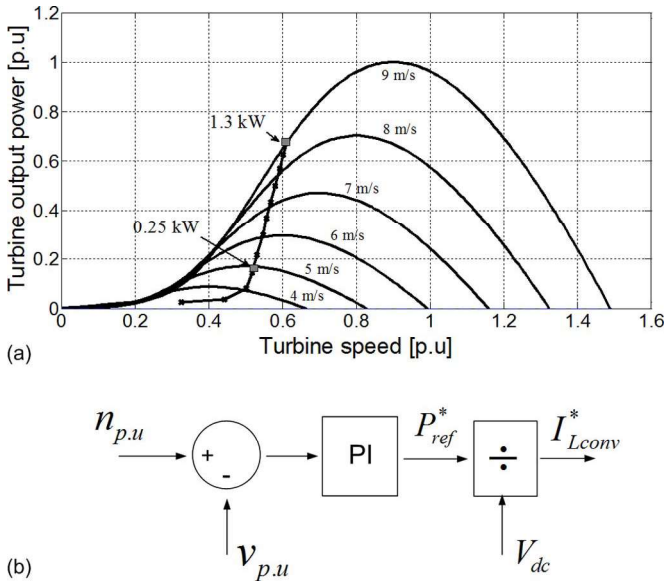

Fig. 4. (a) Wind turbine power characteristics. (b) MPPT control block diagram.

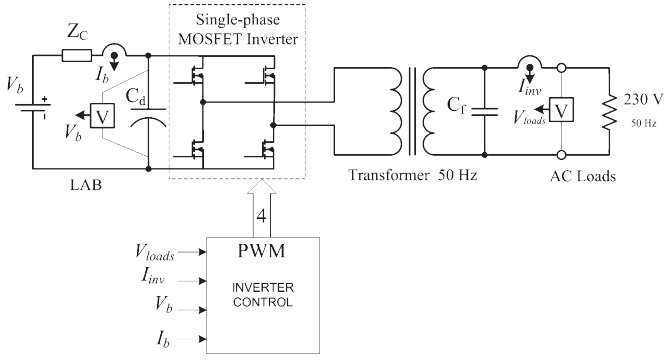

Fig. 5. Storage system configuration.

D. Energy Storage System

The energy storage system is composed of a single-phase MOSFET inverter and a bank of LABs 12 V each (gel type) connected in series to provide the desired value of the inverter battery voltage. The energy storage system configuration is shown in Fig. 5. The LAB is able to supplement the power provided to the load by the wind turbine, when the wind speed is too low.

The equivalent electrical model of the LAB contains a controlled voltage source (E_b), connected in series with the internal resistance $(R_{\rm int})$ and the LAB voltage (V_b). It is known that the E_b voltage depends on the charging state, battery type,

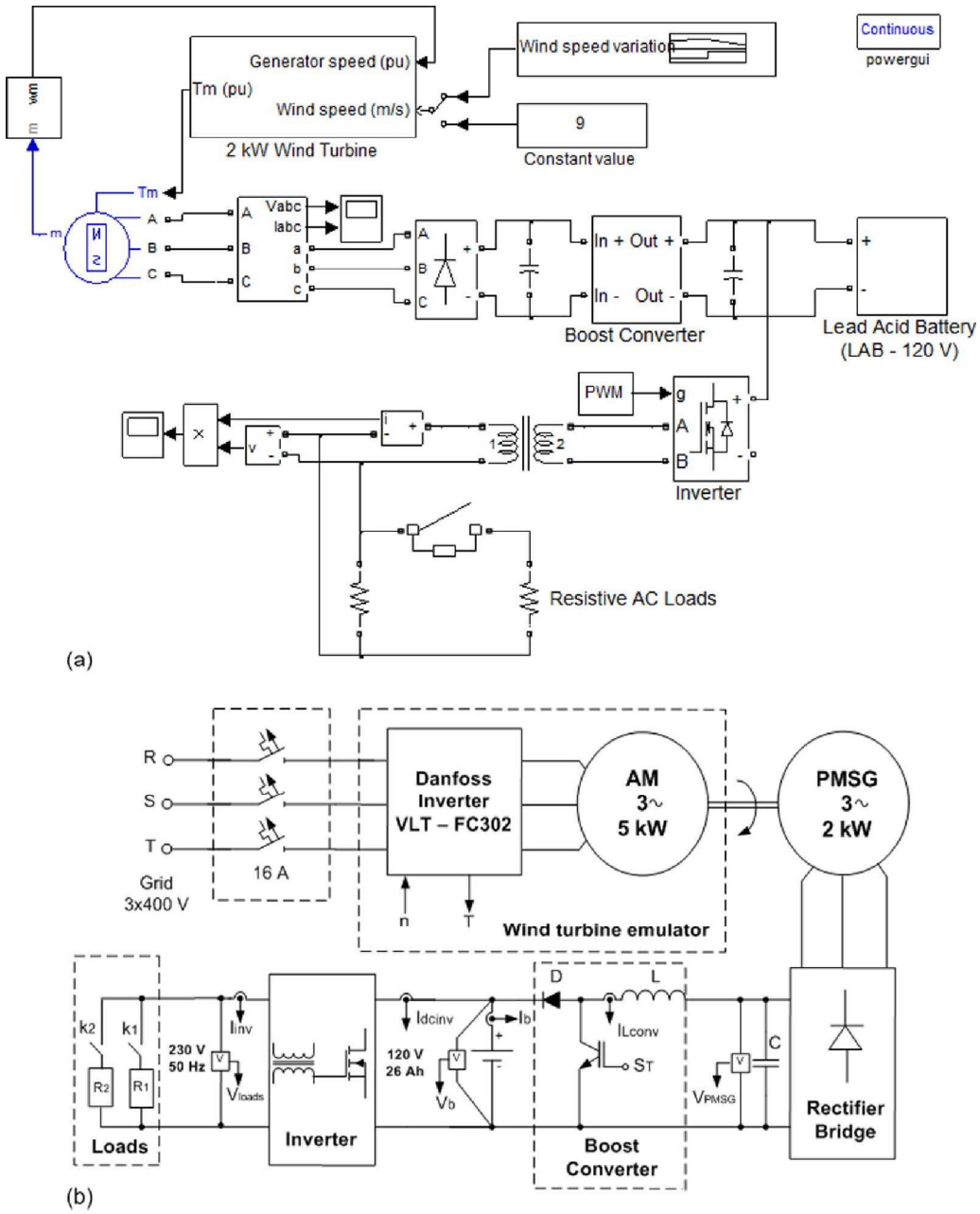

Fig. 6. Implemented structures. (a) Simulink block diagram. (b) Experimental setup.

and temperature, and it is expressed by the following relationship [27]:

$$E_b = E_{b0} - \frac{K \cdot Q}{Q - \int_0^t I_b dt} \tag{7}$$

where E_{b0} is the no-load battery voltage at the rated charge, K is the polarization voltage, Q is the battery capacity, and I_b is the battery current. The input of the charging/discharging controller is used as a parameter—the state of charge (SOC) of LAB and is defined as

$$SOC_{[\%]} = SOC_{0[\%]} + \left(\frac{1}{Q_n} \int_0^t I_b dt \right) \cdot 100 \tag{8}$$

where Q_n is the rated capacity of LAB.

If the LAB is fully charged, $SOC = 1$, and if the battery is discharged at the maximum value, $SOC = SOC_{\min}$. For instance, the maximum recommended discharge for LABs used in such applications is 80%; thus, $SOC_{\min} = 0.2$. As the full discharge is not recommended for LABs, a $SOC_{\min} = 20\%$ will be considered in the regulator's implementation.

The calculation algorithm uses one variable parameter (I_b) and one constant block (Q_n). With a discrete-time integrator block, the mathematical operations, and an initial SOC value, the LAB $SOC_{[\%]}$ is obtained.

III. Simulation and Experimental Results

The proposed system has been modeled and simulated using the Matlab/Simulink/SimPowerSystems environment [28]. Fig. 6 shows the block diagrams for simulation [Fig. 6(a)] and

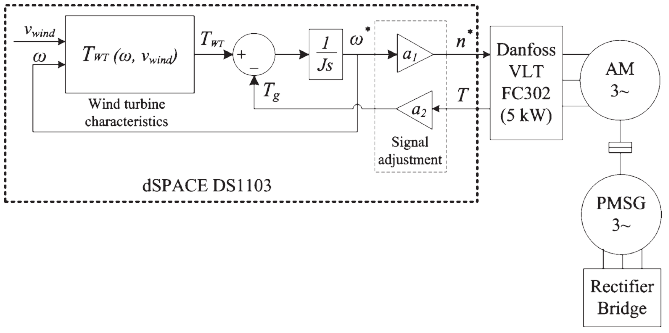

Fig. 7. Wind turbine emulator.

those related to the experimental implementation [Fig. 6(b)]. Measurement blocks are also included.

The experimental results are obtained on a laboratory test bench which includes the described system in conjunction with a wind turbine emulator that drives the PMSG. The PMSG belongs to a real wind turbine. The wind speed changes, and load switching conditions were performed using the wind turbine emulator and a dSPACE DS1103 real-time board. This emulator is able to reproduce the steady and dynamic behavior of a real wind turbine. The hardware scheme is based on a Danfoss VLT FC302 frequency converter, with vector control/open loop torque control, and the real-time control system dSPACE DS1103. Additionally, the theory of real-time control systems is detailed in [29] and [30]. The operating principle is based on a control loop, where the input signal is the electromagnetic torque of the asynchronous motor, and the output signal is the motor speed. The wind speed can be modified through one independent input of the emulator [31]. The block diagram of the wind turbine emulator is shown in Fig. 7.

A graphical user interface has been built, using the control desk software, in order to allow real-time control, evaluation of the system, and finding the desired operating conditions which can verify the studied and proposed cases.

In order to investigate the system's operation, the following simulations and experiments were carried out:

1) variation of the wind speed, while the load is constant (two case studies);
2) load switching, with a fixed wind speed (two case studies).

These will be discussed in the following sections.

A. *Variation of the Wind Speed, While the Load is Constant*

Case 1) Decreasing variation of the wind speed, while the load is constant ($P = 1$ kW).

In Case 1), the entire energy load demand is considered to be 1 kW. The simulation and experimental results for the wind generator are summarized in Fig. 8(a)–(c). During this process, the LAB voltage decreases by about 3 V [Fig. 8(d)]. The simulation and experimental test results for the LAB current are shown in Fig. 8(e). When the LAB is discharging, the battery SOC decreases in order to ensure a stable supply for the loads. The results can be seen in Fig. 8(f). When the wind speed is 5 m/s,

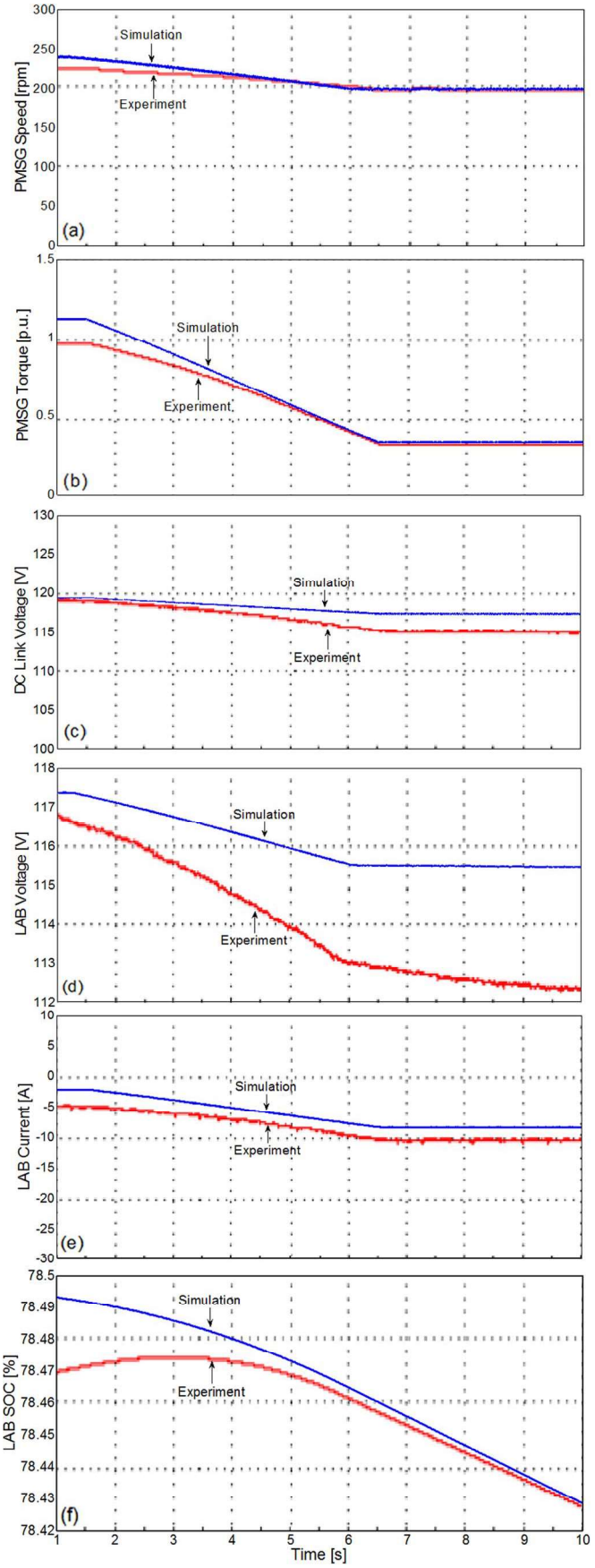

Fig. 8. (a) PMSG rotor speed variation. (b) PMSG electromagnetic torque. (c) DC-link rectifier bridge voltage variation. (d) LAB voltage variation. (e) LAB current variation. (f) LAB-SOC variation.

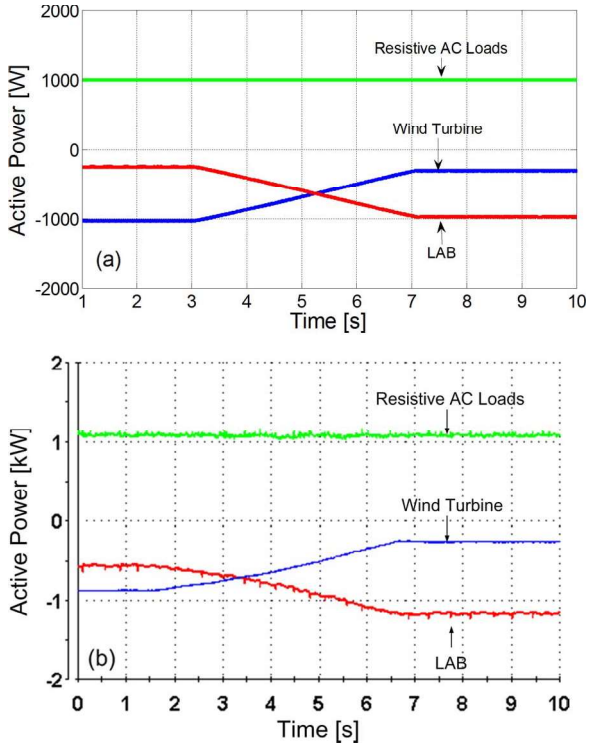

Fig. 9. Active power balance of the system. (a) Simulation. (b) Experiments.

the wind turbine cannot supply the entire energy demand of the load (1 kW); therefore, the battery is supplying the difference. The active power balance of the system is shown in Fig. 9, experimental tests confirming the simulation results.

Case 2) Random wind speed variation with variable load.

In this case, a typical wind profile is implemented, over 100 s, as shown in Fig. 10(a). The profile is based on local wind data characteristics [32]. In a wind-storage system, the battery is smoothening the output power of the wind turbine by charging and discharging accordingly. Corresponding to the two load values which are connected and disconnected [see the waveform in Fig. 10(h)], the experimental results are summarized in Fig. 10(b)–(h).

B. Load Switching, at Fixed Wind Speed (Two Case Studies)

Case 1) 2-kW load switching at 9 m/s;

Case 2) 1-kW load switching at 0 m/s.

In Case 1), the wind speed is maintained constant at 9 m/s. A 2-kW load is connected at $t = 3$ s and disconnected at $t = 7$ s. The simulation and experimental results for the wind turbine emulator are summarized in Fig. 11(a) and (b). The dc-link bridge voltage variation is shown in Fig. 11(c). Furthermore, Fig. 11(d) and (e) shows that the LAB's operating mode changes from charge to discharge during the transient event.

As no load is connected initially, the power difference supplied by the wind turbine is stored in the battery and is then released when the 2-kW load is connected, thus ensuring continuous supply of the load. The SOC slope changes when the load is switched on and off, as shown in Fig. 11(f), which

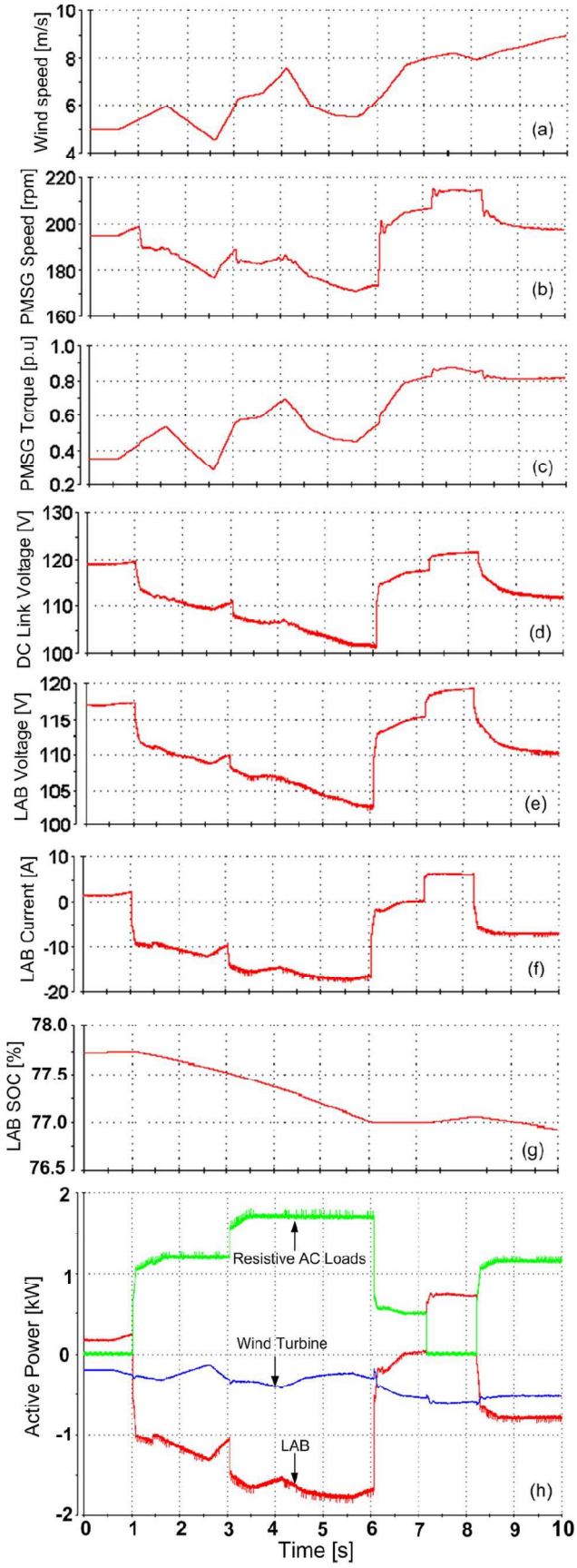

Fig. 10. (a) Typical wind profile for storage device. (b) PMSG rotor speed variation. (c) PMSG electromagnetic torque. (d) DC-link rectifier bridge voltage variation. (e) LAB voltage variation. (f) LAB current variation. (g) LAB-SOC variation. (h) Active power balance of the system.

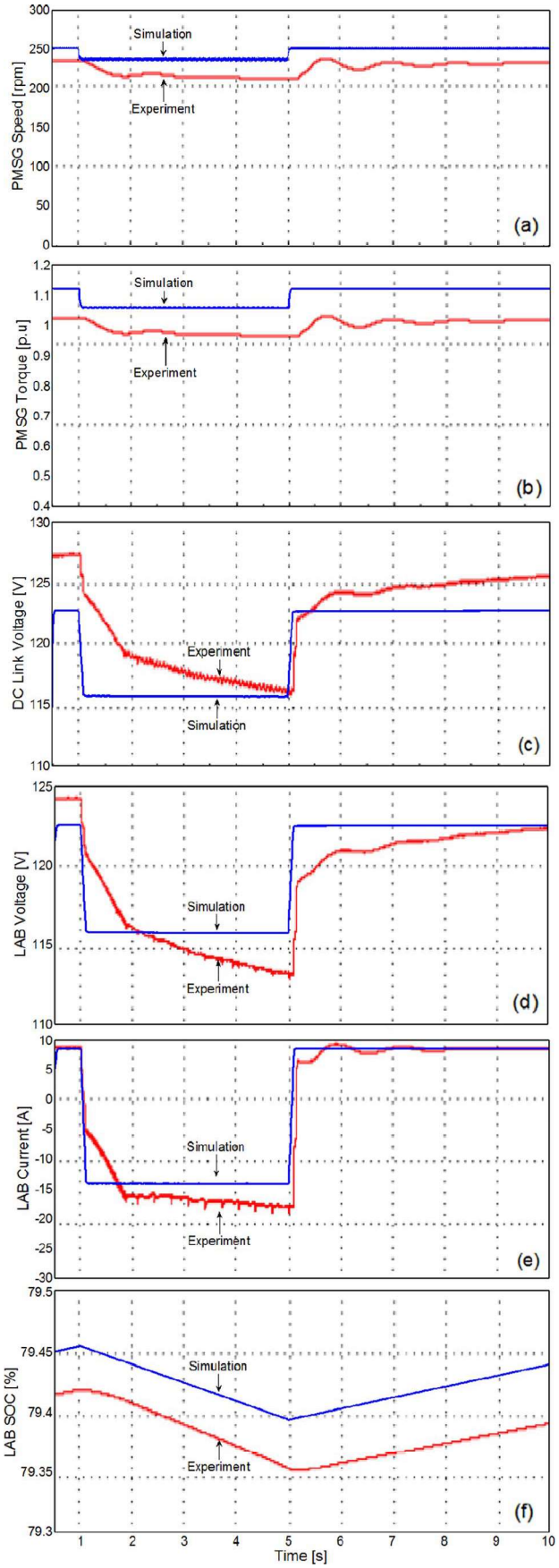

Fig. 11. (a) PMSG rotor speed variation. (b) PMSG electromagnetic torque. (c) DC-link rectifier bridge voltage variation. (d) LAB voltage variation. (e) LAB current variation. (f) LAB-SOC variation.

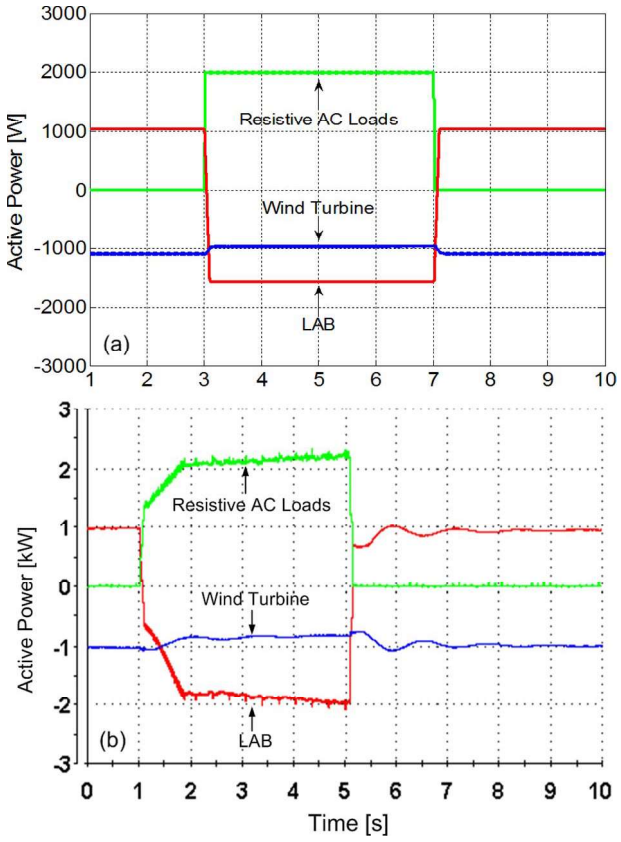

Fig. 12. Active power balance of the system. (a) Simulation. (b) Experiments.

means that the battery is switching from the charging to the discharging modes. Consequently, the system maintains its active power balance (Fig. 12).

In Case 2), the wind turbine does not rotate ($v = 0$ m/s). A 1-kW load is connected at $t = 3$ s, and then, it is disconnected at $t = 7$ s. During the transient event, the LAB voltage decreases [Fig. 13(a)], and the negative current implies that the LAB has entered into the discharge mode, in order to ensure stable supply for the loads [Fig. 13(b) and (c)]. Fig. 14 shows that the active power balance of the system is maintained, regardless of the load change.

Small changes in the battery voltage and current waveforms can be observed on the experimental results, compared with the simulation curves, taken as reference.

The explanation for these differences is that the real system is more complex than the model used in the simulation, and its performance can be affected by many parameters which are not considered in the simulation (the neglected/unknown wires for example).

These differences are more significant in the results presented for load switching [for example, in Figs. 8(d) and 11(d)], due to the use of a real inverter in the laboratory test bench, which has low dynamics during the transient regime, compared with the simulation case, where an ideal inverter is modeled.

In addition, the mismatch of the time axis between the simulation and the experimental test results occurs because of the difficulty of controlling the real system start time, as done in the simulation case.

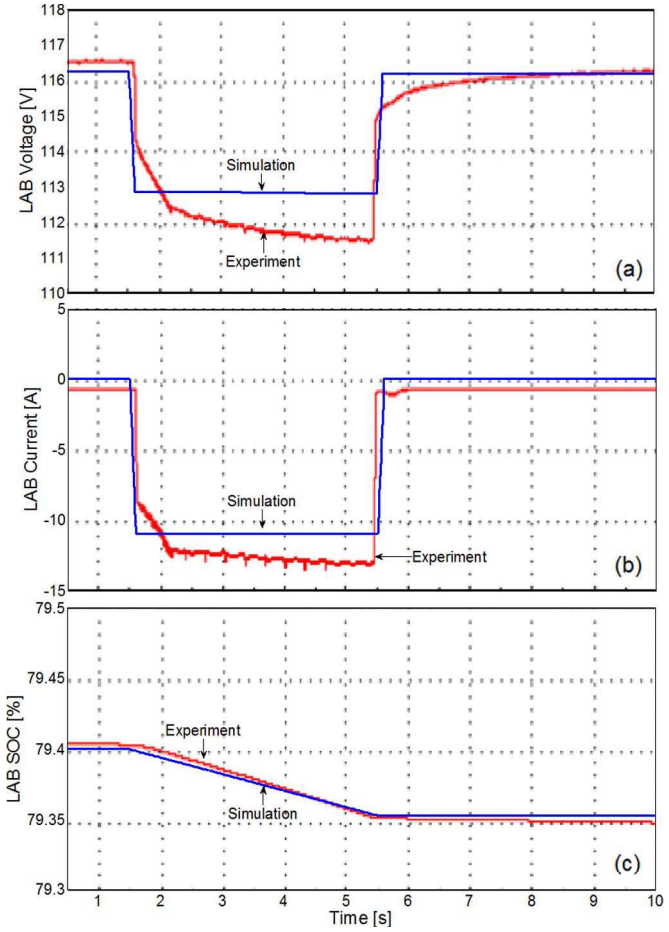

Fig. 13. (a) LAB voltage variation. (b) LAB current variation. (c) LAB-SOC variation.

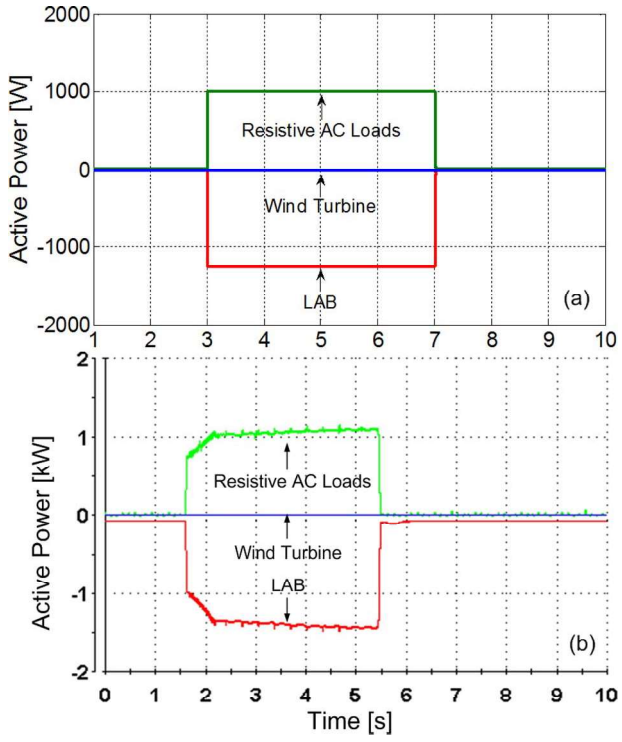

Fig. 14. Active power balance of the system. (a) Simulation. (b) Experiments.

IV. Conclusion

A control structure for single-phase stand-alone wind-based energy sources has been analyzed in this paper. This includes an associated energy storage system, with the role to stabilize the output voltage in autonomous applications.

The main original contributions of this paper are the following: 1) the development of a control topology which achieves MPPT and voltage and battery SOC monitoring, with optimal conditions for battery charging; 2) the design and implementation of a wind turbine emulator with an induction motor and a frequency converter; and 3) the experimental laboratory test bench development to validate in practice the results obtained from simulations.

The MPPT algorithm, which controls the power electronic interface, will ensure a maximum extraction of energy from the available wind. The LAB always ensures the safe supply of the loads (households), regardless of the problems caused by wind speed or load variations, by switching between the charging and the discharging modes.

Simulation and experimental test results show that the active power balance of the system proves to be satisfied during transient loads and variable wind speed conditions.

The configuration can operate with inductive loads, but there is no effect of the L component on the dc-side power circulation, so the specific study of the RL case is of no interest. However, the inverter has to be oversized to bear the reactive component. Thus, the analysis performed and the case studies considered lead to the conclusion that the proposed system can effectively provide reliable and good quality power to the customers in the autonomous power system.

This paper highlights the functionality and efficiency of the control system developed and offers perspectives for future research on autonomous wind energy system control strategies.

References

[1] R. A. Mastromauro, M. Liserre, and A. Dell'Aquila, "Control issues in single-stage photovoltaic systems: MPPT, current and voltage control," *IEEE Trans. Ind. Informat.*, vol. 8, no. 2, pp. 241–254, May 2012.

[2] C. Liu, K. T. Chau, and X. Zhang, "An efficient wind–photovoltaic hybrid generation system using doubly excited permanent-magnet brushless machine," *IEEE Trans. Ind. Electron.*, vol. 57, no. 3, pp. 831–839, Mar. 2010.

[3] M. P. Kazmierkowski, M. Jasinski, and G. Wrona, "DSP-based control of grid-connected power converters operating under grid distortions," *IEEE Trans. Ind. Informat.*, vol. 7, no. 2, pp. 204–211, May 2011.

[4] P. Palensky and D. Dietrich, "Demand side management: Demand response, intelligent energy systems, and smart loads," *IEEE Trans. Ind. Informat.*, vol. 7, no. 3, pp. 381–388, Aug. 2011.

[5] V. C. Gungor, D. Sahin, T. Kocak, S. Ergut, C. Buccella, C. Cecati, and G. P. Hancke, "Smart grid technologies: Communication technologies and standards," *IEEE Trans. Ind. Informat.*, vol. 7, no. 4, pp. 529–539, Nov. 2011.

[6] S. Wencong, H. Eichi, Z. Wente, and M.-Y. Chow, "A survey on the electrification of transportation in a smart grid environment," *IEEE Trans. Ind. Informat.*, vol. 8, no. 1, pp. 1–10, Feb. 2012.

[7] R. Teodorescu, M. Lissere, and P. Rodriguez, *Grid Converter for Photovoltaic and Wind Power Systems*. New York: Wiley, 2011.

[8] E. Monmasson, L. Idkhajine, M. N. Cirstea, I. Bahri, A. Tisan, and M. W. Naouar, "FPGAs in industrial control applications," *IEEE Trans. Ind. Informat.*, vol. 7, no. 2, pp. 224–243, May 2011.

[9] L. S Yang and T. J. Liang, "Analysis and implementation of a novel bidirectional DC–DC converter," *IEEE Trans. Ind. Electron.*, vol. 59, no. 1, pp. 422–434, Jan. 2012.

[10] M. H. Nehrir, C. Wang, K. Strunz, H. Aki, R. Ramakumar, J. Bing, Z. Miao, and Z. Salameh, "A review of hybrid renewable/alternative energy systems for electric power generation: Configurations, control, and applications," *IEEE Trans. Sustain. Energy*, vol. 2, no. 4, pp. 392–402, Oct. 2011.
[11] B. Singh, S. Singh, A. Chandra, and K. Al-Haddad, "Comprehensive study of single-phase AC–DC power factor corrected converters with high-frequency isolation," *IEEE Trans. Ind. Informat.*, vol. 7, no. 4, pp. 540–556, Nov. 2011.
[12] L. Barote and C. Marinescu, "Storage analysis for stand-alone wind energy applications," in *Proc. IEEE OPTIM*, 2010, pp. 1180–1185.
[13] L. Barote, R. Weissbach, R. Teodorescu, C. Marinescu, and M. Cirstea, "Stand-alone wind system with vanadium redox battery energy storage," in *Proc. IEEE OPTIM*, 2008, pp. 407–412.
[14] B. Fleck and M. Huot, "Comparative life-cycle assessment of a small wind turbine for residential off-grid use," *J. Renewable Energy*, vol. 34, no. 12, pp. 2688–2696, Dec. 2009.
[15] M. J. Vasallo, J. M. Andújar, C. Garcia, and J. J. Brey, "A methodology for sizing backup fuel-cell/battery hybrid power systems," *IEEE Trans. Ind. Electron.*, vol. 57, no. 6, pp. 1964–1975, Jun. 2010.
[16] M. Swierczynski, R. Teodorescu, C. N. Rasmussen, P. Rodriguez, and H. Vikelgaard, "Overview of the energy storage systems for wind power integration enhancement," in *Proc. IEEE ISIE*, 2010, pp. 3749–3756.
[17] C. Abbey, L. Wei, and G. Joós, "An online control algorithm for application of a hybrid ESS to a wind–diesel system," *IEEE Trans. Ind. Electron.*, vol. 57, no. 12, pp. 3896–3904, Dec. 2010.
[18] R. C. Harwood, V. S. Manoranjan, and D. B. Edwards, "Lead–acid battery model under discharge with a fast splitting method," *IEEE Trans. Energy Convers.*, vol. 26, no. 4, pp. 1109–1117, Dec. 2011.
[19] T. Ackermann, *Wind Power in Power Systems*. Chichester, U.K.: Wiley, 2005.
[20] Y. Ming, L. Gengyin, Z. Ming, and Z. Chengyong, "Modeling of the wind turbine with a permanent magnet synchronous generator for integration," in *Proc. IEEE Power Eng. Soc. Gen. Meeting*, 2007, pp. 1–6.
[21] I. Boldea, *Variable Speed Generators—The Electric Generators Handbook*. Boca Raton, FL: CRC Press, 2006.
[22] L. G. Gonzalez, E. Figueres, G. Garcera, and O. Carranza, "Synchronization techniques comparison for sensorless control applied to PMSG," in *Proc. ICREPQ*, Apr. 2009, pp. 1–5.
[23] B. Cheng and T. R. Tesch, "Torque feedforward control technique for permanent-magnet synchronous motors," *IEEE Trans. Ind. Electron.*, vol. 57, no. 3, pp. 969–974, Mar. 2010.
[24] Z. Ouyang, O. C. Thomsen, and M. A. E. Andersen, "Optimal design and tradeoff analysis of planar transformer in high-power DC–DC converters," *IEEE Trans. Ind. Electron.*, vol. 59, no. 7, pp. 2800–2810, Jul. 2012.
[25] I. Serban and C. Marinescu, "A sensorless control method for variable-speed small wind turbines," *J. Renewable Energy*, vol. 43, pp. 256–266, Jul. 2012.
[26] S. M. R. Kazmi, H. Goto, H.-J. Guo, and O. Ichinokura, "A novel algorithm for fast and efficient speed-sensorless maximum power point tracking in wind energy conversion systems," *IEEE Trans. Ind. Electron.*, vol. 58, no. 1, pp. 29–36, Jan. 2011.
[27] M. Durr, A. Cruden, S. Gair, and J. R. McDonald, "Dynamic model of a lead acid battery for use in a domestic fuel cell," *J. Power Sources*, vol. 161, pp. 1400–1411, Oct. 2006.
[28] *** SimPowerSystems. [Online]. Available: www.mathworks.com
[29] Y. Chen, C. Yang, and T. Kuo, "Energy-efficient task synchronization for real-time systems," *IEEE Trans. Ind. Informat.*, vol. 6, no. 3, pp. 287–301, Aug. 2010.
[30] Y. Wu, G. Buttazzo, E. Bini, and A. Cervin, "Parameter selection for real-time controllers in resource-constrained systems," *IEEE Trans. Ind. Informat.*, vol. 6, no. 4, pp. 610–620, Nov. 2010.
[31] L. A. C. Lopes, J. Lhuilier, A. mukherjee, and M. F. Khokhar, "A wind turbine emulator that represents the dynamics of the wind turbine rotor and drive train," in *Proc. IEEE PESC*, 2005, pp. 2092–2097.
[32] Historical Weather and Climate Data for Sulina. [Online]. Available: http://www.energymatters.com.au/climate-data/?q=sulina&find=Search

Luminita Barote (M'09) was born in Onesti, Romania, on November 17, 1982. She received the B.S. degree in electrical engineering and computer science, in 2005, the M.S. degree in 2007, and the Ph.D. degree in electrical engineering in 2009 from Transilvania University of Braşov, Braşov, Romania.

She is currently a Researcher with the Department of Electrical Engineering, Faculty of Electrical Engineering and Computer Science, Transilvania University of Braşov. Her current research interests are in the area of renewable energy systems: the control of variable-speed permanent-magnet synchronous and asynchronous generators for small-power wind turbine working in stand-alone system with storage devices (lead–acid battery and vanadium redox flow battery) and also electrical energy storage in a smart microgrid.

Corneliu Marinescu (M'07) was born in Braşov, Romania, on May 26, 1948. He received the Dipl.Ing. degree in electromechanical engineering from the Polytechnic Institute of Braşov, Braşov, in 1971 and the Ph.D. degree from the Politehnica University of Bucharest, Bucharest, Romania, in 1991.

He is currently a Full Professor with the Department of Electrotechnics, Faculty of Electrical Engineering and Computers Science, Transilvania University of Braşov, where he is also the Head of Power Electronics and Electrical Machines (POWERELMA) research laboratory. He is the author or coauthor of more than 160 journal/conference papers in his research fields. His areas of interests include power electronics applied to renewable energy sources.

Marcian N. Cirstea (M'97–SM'04) received the B.S. degree in electrical engineering from Transilvania University of Braşov, Braşov, Romania, and the Ph.D. degree from the Nottingham Trent University, Nottingham, U.K., in 1996.

He is currently a Professor of industrial electronics and the Head of the Department of Computing and Technology, Anglia Ruskin University, Cambridge, U.K., after previously working with De Montfort University, Leicester, U.K. He has coauthored several technical books and over 120 peer-reviewed papers, three of which have received awards. His research is focused on digital controllers for power electronics.

Dr. Cirstea has delivered six international tutorials on *VHDL Design for Power Electronic Systems Modeling and FPGA Controller Prototyping*. He is the Founder and Past Chairman of the "Electronic Systems on Chip" Technical Committee of IEEE Industrial Electronics Society, a Fellow of The Institution of Engineering and Technology (IET) and a Chartered Engineer. He is an Associate Editor for IEEE TRANSACTIONS ON INDUSTRIAL ELECTRONICS/IEEE TRANSACTIONS ON INDUSTRIAL INFORMATICS and was the General Chair of IEEE conferences (2008 International Symposium on Industrial Electronics (ISIE), Cambridge, and 2012 Optimization of Electrical and Electronic Equipments (OPTIM), Braşov). He has coordinated a European renewable energy project consortium.